Realization of introducing a non-woven veil on the interlaminar radial strength of glass-epoxy L-bend composites

P. S. Shivakumar Gouda*
Department of Aeronautical Engineering, Dayananda Sagar College of Engineering, Bengaluru - 560078 Karnataka, India.
ursshivu@gmail.com

Vinayak S. Uppin, I. Sridhar
Research Center, Department of Mechanical Engineering, SDM College of Engineering & Technology, Dharwad, Visvesvaraya Technological University, Belagavi, Karnataka, India.
ursuppin@gmail.com, sridhari74@gmail.com,

Gururaj Hatti
Department of Mechanical Engineering, KLS Vishwanathrao Deshpande Institute of Technology, Haliyal, Visvesvaraya Technological University, Belagavi, Karnataka, India.
hatti.gururaj@gmail.com

M. A. Umarfarooq
Center for Material Science, Karpagam Academy of Higher Education, Coimbatore, Tamil Nadu 641 021, India
Department of Mechanical Engineering, Karpagam Academy of Higher Education, Coimbatore, Tamil Nadu 641 021, India
umarfarooq.ma@gmail.com

Aravind Muddebihal
Research Center, Department of Mechanical Engineering, SDM College of Engineering & Technology, Dharwad, Visvesvaraya Technological University, Belagavi, Karnataka, India.
Department of Mechanical Engineering, Angadi Institute of Technology & Management, Belagavi, Visvesvaraya Technological University, Belagavi, Karnataka, India.
aravindbm21@gmail.com

K.N. Bharath
G.M. Institute of Technology, Davangere, Visvesvaraya Technological University, Belagavi, Karnataka, India.
kn.bharath@gmail.com

Abhilash Edacherian
Department of Mechanical Engineering, College of Engineering, King Khalid University, Abha, Saudi Arabia
edalheriad@kku.edu.sa

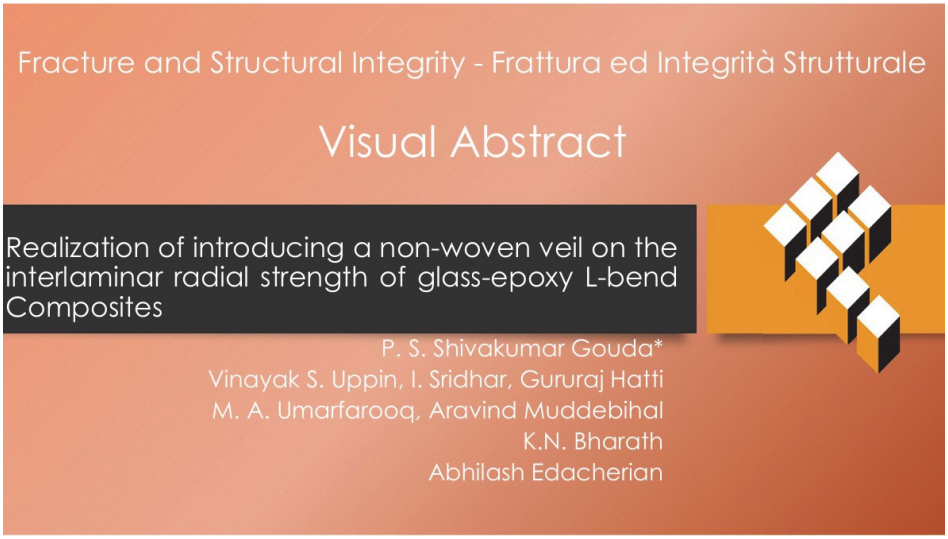

Citation: Shivakumar Gouda, P.S., Uppin, V. S., Sridhar, I., Hatti, G., Umarfarooq, M. A., Muddebihal, A., Bharath, K. N., Edacherian, A., Realization of introducing a non-woven veil on the interlaminar radial strength of glass-epoxy L-bend composites, Fracture and Structural Integrity, 75 (2026) 76-87.

Received: 21.08.2025
Accepted: 30.09.2025
Published: 16.10.2025
Issue: 01.2026

KEYWORDS. Non-woven veils, Curved beam, Curved beam strength, Interlaminar radial stress, Delamination mitigation.

INTRODUCTION

Fiber-reinforced polymer (FRP) composites are gaining popularity due to their superior specific strength, stiffness, corrosion resistance, fatigue life, and manufacturing flexibility. These remarkable features facilitate the production of lightweight, intricate structural components such as L, T, and C-shaped configurations using FRP composites[1,2]. Such designs are frequently employed to connect perpendicular sections in aircraft wings, tails, and wind turbine blades [3]. However, these components are vulnerable to delamination failure through the thickness, particularly in curved regions, due to insufficient reinforcement in the thickness direction. Therefore, enhancing interlaminar properties in curved regions is crucial for ensuring reliable and safe composite structures.

Many researchers have conducted experiments to enhance the strength of curved laminates by preventing or delaying delamination under service loads. Ranz et al.[4] reported that using the tufting technique (inserting threads through the thickness) with a density of 5×5 mm can significantly improve ILRS by approximately 40% in four-layered composites. Ju et al.[5] studied the impact of stainless-steel Z-pins reinforced at the curved region of CFRP L-bends, with a range of pin diameters and densities, on CBS. Their research revealed that a pin diameter of 0.3 mm with a surface areal density of 2.0% led to a notable improvement of about 42% in CBS. This enhancement was attributed to the smaller resin-rich zones around the pins and reduced fiber damage compared to laminates with larger-diameter pins. Babu et al.[3] conducted experiments to enhance CBS and ILTS by reinforcing short glass fiber patches and stitching aramid filaments through the thickness. All these methods demonstrated notable improvements in CBS and ILTS. Remarkably, single stitching of aramid fibers at the corners showed the greatest improvement compared to other reinforcing methods and baseline composites. Although reinforcing fibers through the thickness can improve out-of-plane properties, careful consideration is necessary to mitigate any adverse impact of fiber-rich zones on in-plane mechanical properties[6].

Similarly, reinforcing fillers into FRP composites can improve delamination resistance without significantly compromising in-plane mechanical properties [7–9]. Additionally, the thickness of the curved laminate and the weight percentage (wt%) of recycled milled glass fibers significantly influence CBS and ILTS in GFRP composites[10]. Gouda et al.[11] incorporated various fillers, including multi-walled carbon nanotubes (MWCNTs), aluminum oxide (Al_2O_3), and silicon carbide (SiC), in proportions ranging from 0.5 to 2 wt%, at the interface of curved glass lamina using the drawdown coating technique. Among all the fillers, the specimen loaded with 0.5 wt% SiC exhibited a significant enhancement in both CBS and ILRS compared to other filler-loaded and reference specimens. Gumgol et al.[12] performed experiments to examine how short kenaf fibers and graphene oxide (GO) reinforcement affect the ILRS of GFRP curved composite laminates. They reported

that incorporating kenaf fiber at 7.5 wt% significantly improved ILRS by approximately 78%. Conversely, GO reinforcement had a detrimental effect on ILRS. Additionally, the same authors found that reinforcing 7.5 wt% cellulose resulted in a 31% improvement in ILRS [13]. Moreover, Avalon et al.[14] conducted both experimental and numerical investigations on the strength and failure modes of CFRP curved beams. They explored the effects of adding vapor-grown carbon nanofibers to the epoxy resin matrix by varying the bending angle radius and laminate thickness. The authors emphasized that incorporating these nanofibers significantly mitigated the risk of catastrophic failure. One of the main challenges in using micro- and nano-fillers is achieving uniform dispersion. For example, CNT-reinforced CFRP composites showed a favorable impact on Mode-I and Mode-II IFT, but an adverse effect on curved beam radial stresses [15].
Besides, Benjamin L. et al.[16] successfully interleaved carbon nanotube (CNT) sheets in CFRP composites, leading to a significant improvement—about 42%—in interlaminar tensile strength (ILT) compared to baseline specimens. This demonstrates that, when dispersion challenges are overcome, the inclusion of nanofillers can markedly enhance composite material properties. Furthermore, IFT under both opening and shear modes was improved by incorporating various non-woven veils interleaved within the composite [17–23]. Studies suggest that this method can be highly effective in enhancing interlaminar properties, particularly in the curved regions of composite laminates.
This research investigates the impact of veil interleaving and its areal density on L-bend curved beams by evaluating their CBS and ILRS. Carbon veils with areal densities of 15, 20, and 30 g/m^2, and glass veils with 25 and 30 g/m^2, were used for interleaving. Both interleaved and non-interleaved L-bend composite laminates were fabricated using hand layup and compression moulding techniques. The CBS and ILRS of the curved beams were tested via a four-point bending test. The following sections provide comprehensive details on the materials, manufacturing techniques, and testing procedures employed in this study.

EXPERIMENTAL

Materials

Unidirectional glass fabric was used as the reinforcement, and epoxy resin (Araldite LY 556) with hardener (HY 951) served as the matrix material to develop L-bend composite laminates. Non-woven veils such as 15, 20, and 30 g/m^2 carbon, and 25 and 30 g/m^2 glass veils were used as interleaving materials, which are supplied by Essen International, India. The length of 6 and 12 mm fibers was used to construct both nonwoven veils. The carbon and glass fiber in the veils have a diameter of 7 and 11 μm, respectively.

Manufacturing of curved laminates

The manufacturing of L-bend composite laminates, both non-interleaved and interleaved, was carried out using the hand layup technique followed by compression moulding. Fig. 1 illustrates the various steps involved in the fabrication process. Initially, a mould release agent was sprayed onto the surface of the metal moulds, wiped using a cotton cloth, and allowed to dry for 10 minutes to facilitate easy demoulding after curing. Next, the fabric was placed on the bottom tool plate, and resin was uniformly applied using a paintbrush. Subsequently, the next fabric layer was placed, and a roller was used to eliminate entrapped air. The non-interleaved composite laminate was fabricated by stacking glass fabrics in a $[0]_{16}$ orientation. To evaluate the effect of modification in a specified zone [24] a thin copper wire (0.2mm) was inserted at the mid-plane within the curved region, i.e., between the 8th and 9th layers, serving as a crack initiator, as shown in Fig. 2(a). A similar procedure was followed to fabricate the veil-interleaved samples, wherein a non-woven veil was interleaved between the 8th and 9th layers, as depicted in Fig. 2(b). Subsequently, the top tool plate was placed, and the assembly was cured in a compression moulding machine at a temperature of 120 °C for 10 minutes. Finally, the cured laminate edges were trimmed, and sample codes were marked, with their descriptions provided in Tab. 1.

Sample Code	Description
GEC	Non-interleaved glass epoxy composite
GEC-15C	15 g/m^2 non-woven carbon veil interleaved glass epoxy composite
GEC-20C	20 g/m^2 non-woven carbon veil interleaved glass epoxy composite
GEC-30C	30 g/m^2 non-woven carbon veil interleaved glass epoxy composite
GEC-25G	25 g/m^2 non-woven glass veil interleaved with glass epoxy composite
GEC-30G	30 g/m^2 non-woven glass veil interleaved with glass epoxy composite

Table 1: Sample codes and their description.

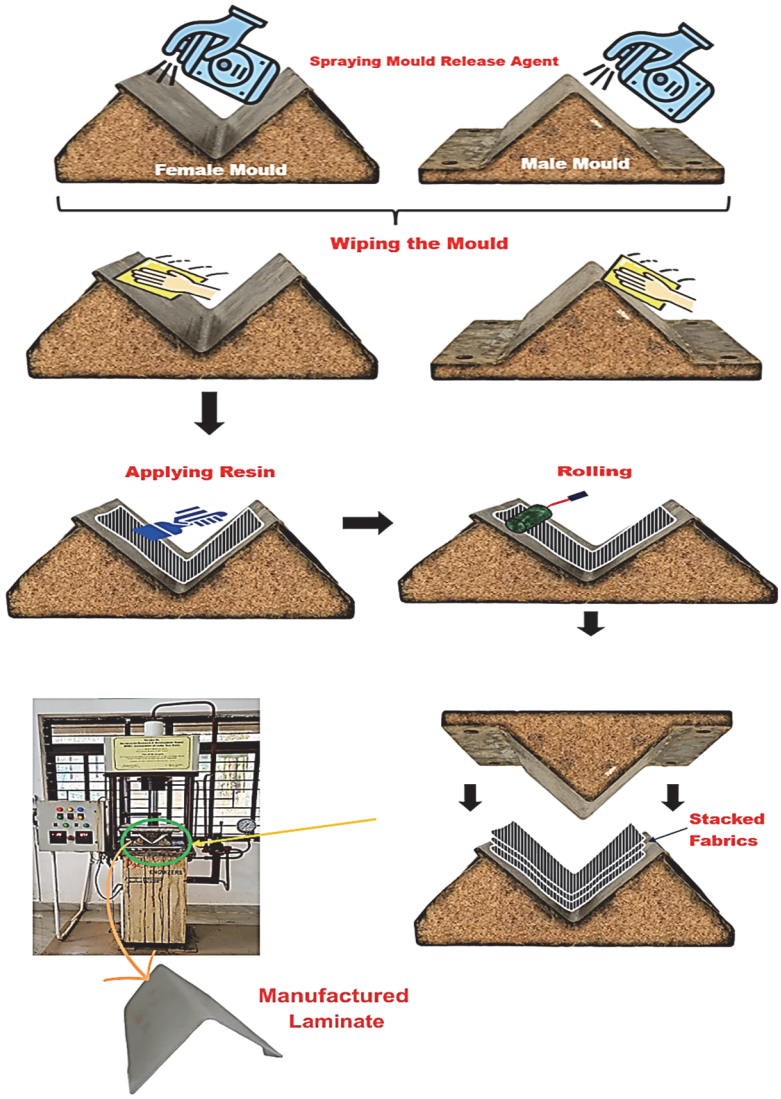

Figure 1: Schematic representation of the laminate manufacturing process of L Bend composite Laminate.

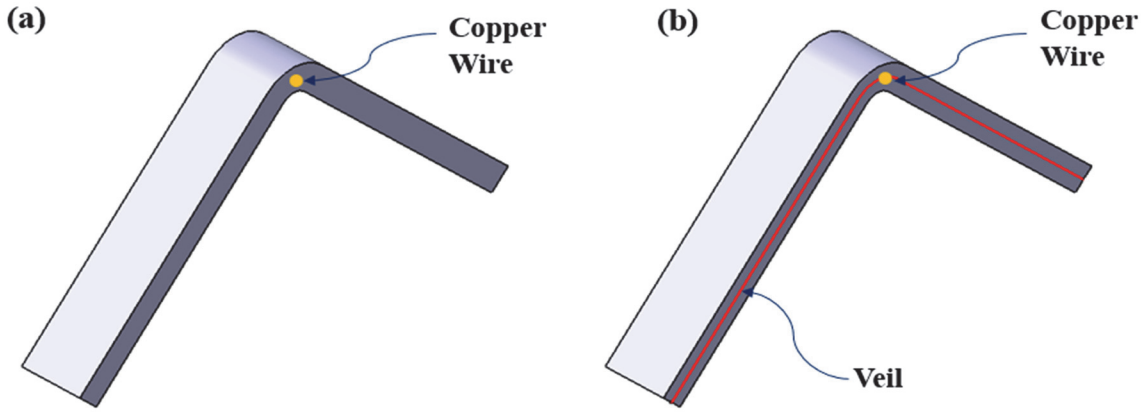

Figure 2: Schematic representation of L-bend laminate (a) non-interleaved, and (b) non-woven veil Interleaved

Four-point bending test

The delamination threshold stress in L-bend composites was determined using a four-point bending test in accordance with ASTM D6415 [25]. The dimensional parameters of the L-bend laminate are illustrated in Fig. 3(a). The positioning of the specimen in the four-point bending fixture, corresponding to the loading and support points, is shown in Fig. 3(b). The specimen loaded in the fixture and placed in the universal testing machine (UTM) is shown in Fig. 3(c). A constant crosshead displacement rate of 1 mm/min was applied to the L-bend laminate through the top rollers. The load was applied until a sudden drop in the load was observed. Five samples were tested for each composition, and the mean values along with their standard deviation were evaluated.

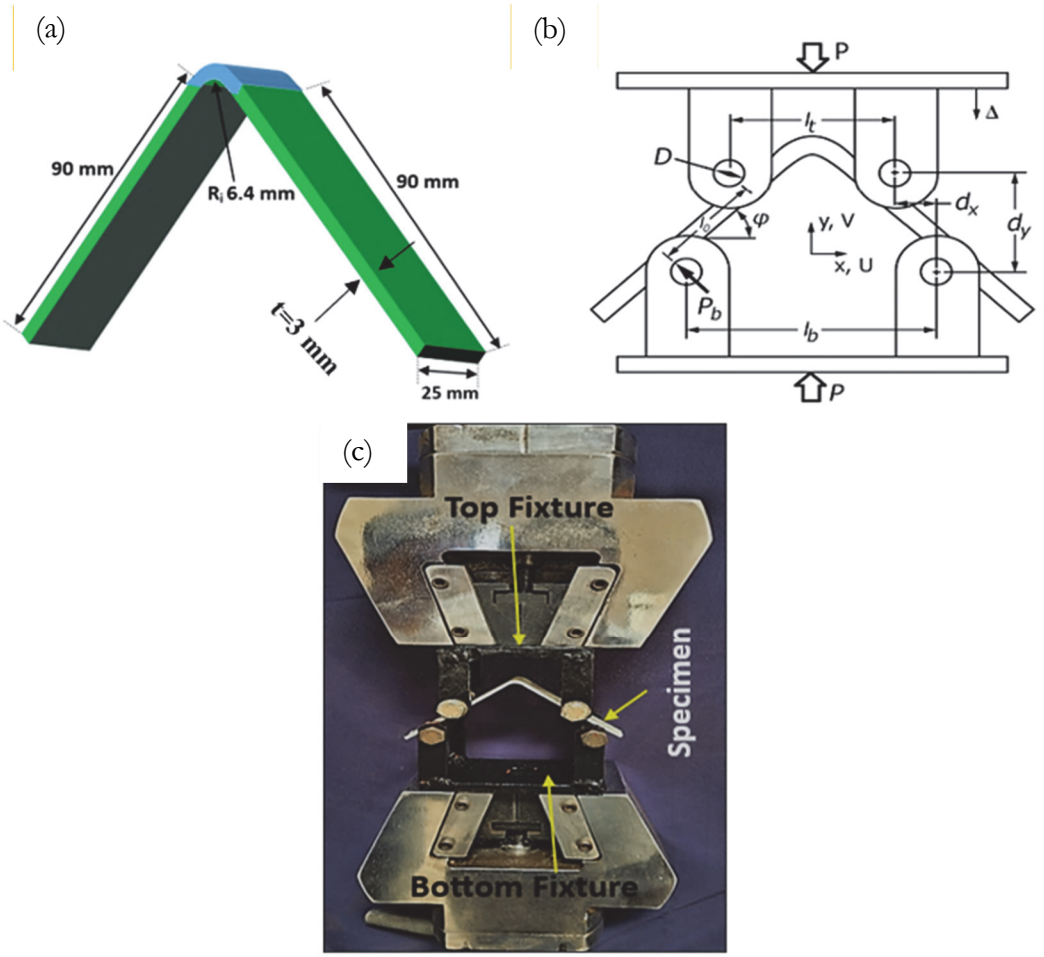

Figure 3: (a) L-bend laminate dimensions (b) Four-point bending fixture as per ASTM D 6415 and (c) Four-point bending fixture and loaded specimen in UTM

The CBS was calculated using Eqn. (1), with the corresponding load at which delamination initiated in the curved region of the laminate. Lekhnitskii [26] developed the equation for ILRS under pure bending, which was calculated using Eqns. (2)-(6).

$$CBS = \frac{M}{w} = \left(\frac{P}{2w\cos\varnothing}\right)\left(\left(\frac{d_x}{\cos\varnothing}\right) + (D+t)\tan\varnothing\right) \tag{1}$$

$$\sigma_r = -\left(\frac{CBS}{r_0^2 g}\right)\left[1 - \frac{(1-\varrho^{k+1})}{(1-\varrho^{2k})}\left(\frac{r_m}{r_0}\right)^{k-1} - \frac{(1-\varrho^{k-1})}{(1-\varrho^{2k})}\varrho^{k+1}\left(\frac{r_0}{r_m}\right)^{k+1}\right] \tag{2}$$

where,

$$\varrho = \frac{r_i}{r_0} \tag{3}$$

$$k = \sqrt{\frac{E_\theta}{E_r}} \tag{4}$$

$$g = \frac{1-\varrho^2}{2} - \frac{k}{k+1}\frac{\left(1-\varrho^{k+1}\right)^2}{1-\varrho^{2k}} + \frac{k\varrho^2}{k-1}\frac{\left(1-\varrho^{k-1}\right)^2}{1-\varrho^{2k}} \tag{5}$$

$$r_m = \left[\frac{(1-\varrho^{k-1})(k+1)(\varrho r_o)^{k+1}}{(1-\varrho^{k+1})(k-1)(r_o)^{-(k-1)}}\right]^{\frac{1}{2k}} \tag{6}$$

where 'M' denotes bending moment; 't' denotes thickness and 'w' denote width of the L-bend specimen; 'P' is the applied load; 'dx' and 'dy' are horizontal and vertical distances between the rollers on either side of the bending fixture, respectively; 'Ø' refers to the angle between horizontal reference line and the specimen leg; D is diameter of the cylindrical loading bars on the four-point-bending fixture; 'r_o' and 'r_i' are the outer and inner radii of curved section in L-bend laminates; 'r_m' indicates the radial position at the maximum interlaminar (radial) tensile stress; 'ρ', 'k', and 'g' are parameters used in strength calculations; and 'σ_r' represents the radial stress in curved section. 'E_r' and 'E_θ' are the elastic moduli in radial and tangential directions, respectively.

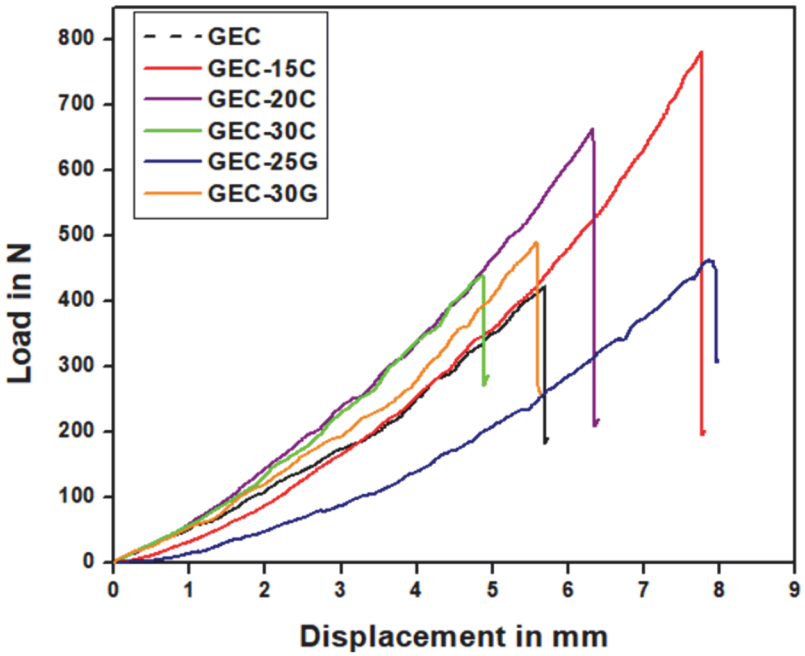

Figure 4: Load-displacement response curves L-bend composite laminates.

RESULTS AND DISCUSSIONS

Curved beam strength and Interlaminar radial stress

Fig. 4 depicts the mean applied load versus displacement curves for non-woven veil interleaved and non-interleaved glass/epoxy composites obtained from a four-point bending test. The samples exhibited elastic bending behavior up to their respective maximum loads. The bending characteristics were influenced by the areal density and the type of non-woven veil used in the composite. After reaching the maximum load, a sharp drop in load was observed, indicating

delamination between the plies. Furthermore, composites interleaved with higher veil areal density exhibited slightly higher stiffness compared to those interleaved with lower veil areal density. The plain (non-interleaved) specimen showed a maximum load of 422 N. The maximum loads for the non-woven veil interleaved samples GEC-15C, GEC-20C, GEC-30C, GEC-25G, and GEC-30G were 782 N, 664 N, 441 N, 462 N, and 491 N, respectively. These results indicate that for carbon veil interleaved samples, the load-carrying capacity decreases as the areal density increases. Conversely, for glass veil interleaved samples, the load-carrying capacity increases with increasing areal density.

The values of CBS for both non-woven veil interleaved and non-interleaved composite samples are presented in Fig. 5. The CBS for the non-interleaved reference sample was approximately 710 N-mm/mm. In contrast, the maximum CBS values for the non-woven veil interleaved samples GEC-15C, GEC-20C, GEC-30C, GEC-25G, and GEC-30G were 1335, 1129, 753, 780, and 832 N-mm/mm, respectively. This corresponds to improvements of approximately 88%, 59%, 6%, 9%, and 17%, respectively, compared to the non-interleaved sample. Furthermore, as shown in Fig. 5, an increase in the areal density of the carbon veil from 15 to 30 g/m² led to a significant reduction in CBS of approximately 43%. This behavior may be attributed to the increased areal density, which hinders proper bonding between adjacent laminate layers, as well as the limited deformability of the carbon fibers within the interleaf during crack propagation. This reduced the effectiveness of the veil, leading to premature and critical delamination between the plies. Conversely, a moderate improvement of about 6% in CBS was observed in the glass veil interleaved samples when the areal density increased from 25 to 30 g/m². This enhancement may be due to the greater deformability of lower-stiffness glass fibers compared to carbon fibers, which allows better energy absorption and stress distribution during crack propagation.

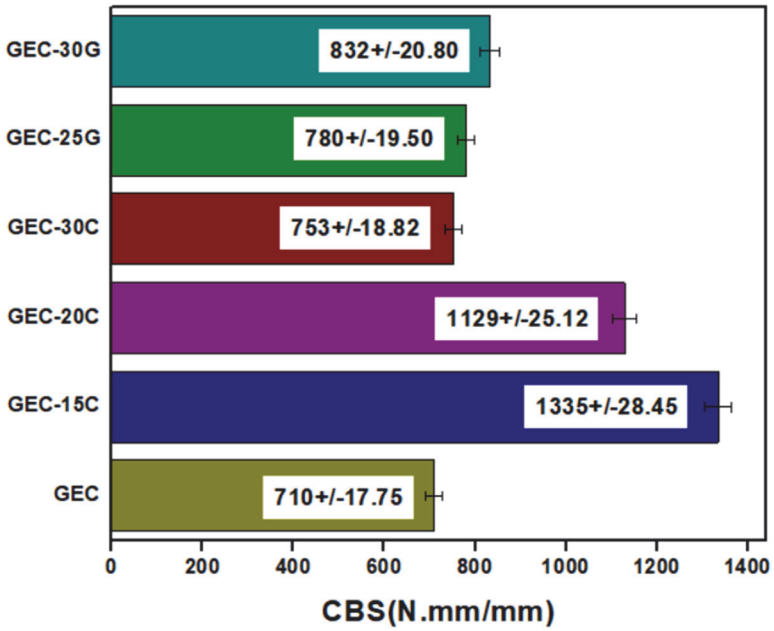

Figure 5: CBS values of L-Bend composite laminates.

Fig. 6 depicts the ILRS of non-woven veil interleaved and non-interleaved composite samples. A notable improvement in ILRS was observed for all veil-interleaved samples, except for the 30 g/m² carbon veil. From Fig. 6, it can be seen that the maximum improvements in radial stress were approximately 57% and 7% for the 15 g/m² carbon and 30 g/m² glass veil interleaved samples, respectively, in comparison to the non-interleaved sample. However, as the areal density of the carbon veil increased from 15 to 30 g/m², a significant reduction of about 43% in radial stress was observed. In contrast, increasing the areal density of the glass veil from 25 to 30 g/m² resulted in no significant variation in radial strength. Through-thickness failure modes for the tested samples are shown in Fig. 7. For the plain specimen, multiple delamination's above and below the pre-crack location indicate rapid crack propagation through the thickness of the composite (Fig. 7(a)). In the 15 g/m² carbon veil interleaved sample, a cohesive failure zone was observed, resulting in the highest load-bearing capacity. This suggests that the crack followed a more tortuous path (Fig. 7(b)). However, as the areal density of the carbon veil increased to 20 and 30 g/m², adjacent layer delamination's were observed (Figs. 7(c) and 7(d)). This behavior may be attributed to reduced flexibility of the interleaf, which caused localized stress concentrations and premature failure under loading. For the glass veil interleaved samples (25 and 30 G/M2), multiple delamination's were also observed. Nevertheless, the deformability of the lower-stiffness glass fibers contributed to an improvement in the CBS of the composite (Figs. 7(e) and 7(f)).

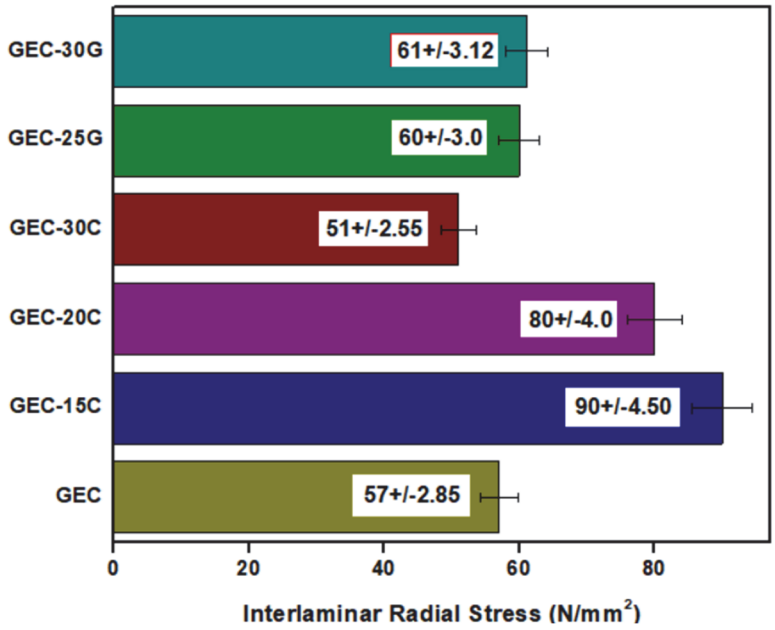

Figure 6: ILRS values of L-Bend composite.

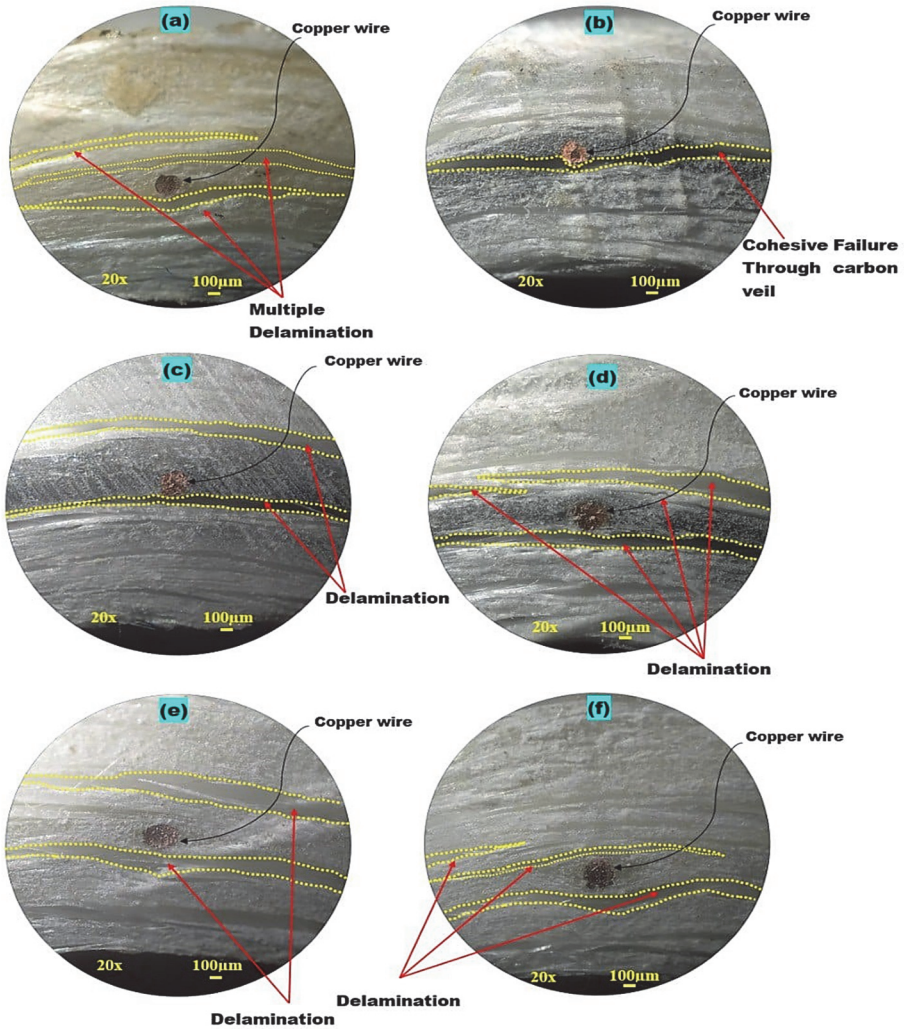

Figure 7: High resolution camera photo images at the curved region of L-bend (a) GEC (b) GEC-15C (c) GEC-20C (d) GEC-30C (e) GEC-25G and (f) GEC-30G.

Statistical analysis of interlaminar radial stresses

A t-test is a statistical analysis test used to determine whether there is a significant difference between the means of two groups. To determine the statistical significance of the observed differences in ILRS, independent sample t-tests were performed between the baseline GEC and each veil-interleaved configuration. The tests were carried out at a 95% confidence level ($\alpha = 0.05$). The results (Tab. 2) revealed that GEC-15C and GEC-20C exhibited highly significant improvements in ILRS compared to baseline ($p < 0.001$). However, the GEC-30C showed a significant reduction in ILRS ($p = 0.0081$), confirming that higher carbon veil areal density diminishes performance. For the glass veil interleaved laminates, differences were not statistically significant. The GEC-25G showed only a marginal increase ($p = 0.1437$), while GEC-30G also exhibited slight improvement but did not meet the significance threshold. Overall, the analysis confirms that low areal density carbon veils (15 – 20 g/m²) significantly enhances ILRS, whereas high areal density carbon veils (30 g/m²) reduce them, and glass veils provide only non-significant improvements. These statistical findings align with the experimental trends and confirm that the effectiveness of veil interleaving is highly influenced by both the fiber type and its areal density.

Comparison	t-statistic	p-value	Significance
GEC vs GEC-15C	13.85	< 0.001	Significant
GEC vs GEC-20C	10.47	< 0.001	Significant
GEC vs GEC-30C	-3.51	0.0081	Significant
GEC vs GEC-25G	1.62	0.1437	Not significant
GEC vs GEC-30G	2.12	0.0675	Not significant

Table 2: Statistical analysis of ILRS.

Analysis of SEM images

SEM analysis was conducted to investigate the failure mechanisms in both interleaved and non-interleaved composite samples. Fig. 8(a) illustrates that the glass fibers were loosely attached to the matrix, indicating a weak interfacial bond between the fiber and matrix. In contrast, the 15 g/m² carbon veil interleaved sample, shown in Fig. 8(b), exhibited notable features such as matrix deformation, river lines, and fibers embedded within the matrix. These observations suggest a robust interfacial bond between the veil and the glass fabric [27]. The micrographs of the 20 and 30 g/m² carbon veil interleaved samples, presented in Figs. 8(c) and 8(d), revealed evidence of fiber traces, matrix cracking, fiber fracture, and crushing of both fiber and matrix. Upon multiple delamination failures, different failure such as fiber fracture, debonding between the fibers, and crushing of the matrix was noticed, which indicates the rapid growth of the crack [3,10]. Figs. 8(e) and 8(f) illustrate fiber traces, matrix deformation, tide marks, hackles, and fiber embedding within the matrix, all of which are indicative of effective interaction between the non-woven veils and the surrounding glass fabric layers.

CONCLUSIONS

The effect of non-woven veil interleaving and its areal density on CBS and ILRS in glass epoxy L-bend laminates was experimentally investigated. In this study, both interleaved and non-interleaved laminates were successfully fabricated by introducing a crack initiator using the hand lay-up method, followed by compression moulding. Critical radial stresses were determined by conducting four-point bending tests on the curved L-bend composites. The interleaving of non-woven carbon and glass veils significantly influenced the load-bearing capacity of the L-bend laminates. As the areal density of the carbon veil increased from 15 to 30 g/m², a decrease in load-bearing capacity was observed. In contrast, an improvement was noted when the areal density of the glass veil increased from 25 to 30 g/m². CBS was notably affected by both the type and the areal density of the interleaving material. Maximum improvements of approximately 88% and 17% were observed for the 15 g/m² carbon and 30 g/m² glass veil interleaved samples, respectively. For high-modulus fiber (carbon) veil interleaved samples, higher areal density led to a reduction in CBS due to poor flexibility and bonding. On the other hand, in low-modulus fiber (glass) veil interleaved samples, CBS improved with increasing areal density, likely due to better deformation ability and interface bonding. ILRS was found to be highly dependent on both the areal density and the type of veil. For high-modulus veil interleaving, lower g/m² veils provided better performance, attributed to enhanced bonding with the glass fabric. In contrast, for low-modulus veil interleaving, only minor variations in ILRS were observed with changing areal density. SEM analysis revealed key fracture patterns supporting the presence of improved interfacial bonding between the veil and the glass fabric, which helped resist early delamination. Features such as matrix deformation,

hackles, and fibers embedded in the matrix were noted, contributing to the enhancement of ILRS. These features varied according to the areal density of the veil materials.

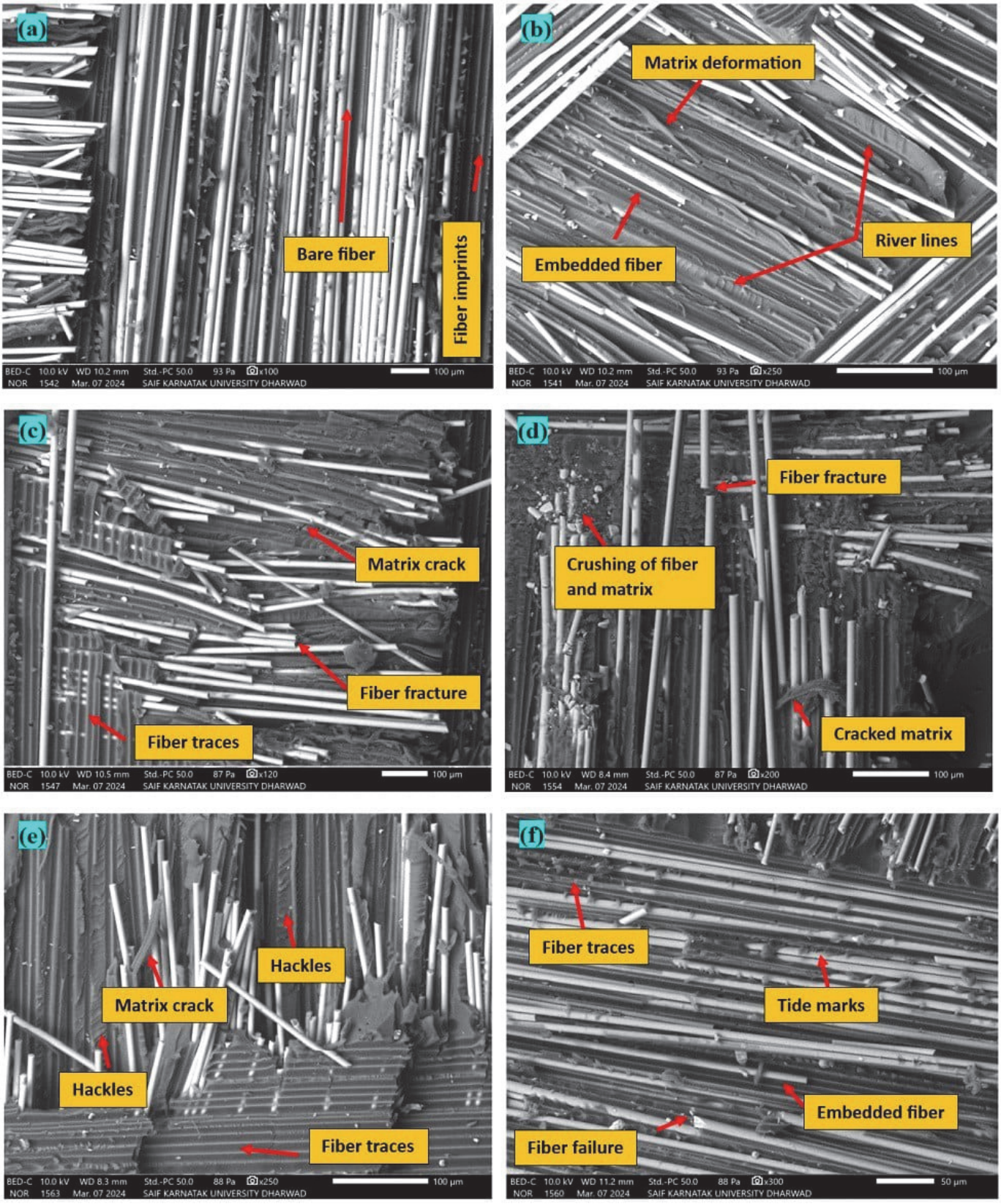

Figure 8: SEM images of a fractured sample (a) GEC (b) GEC-15C (c) GEC-20C (d) GEC-30C (e) GEC-25G and (f) GEC-30G.

ACKNOWLEDGMENT

The authors would like to express their sincere gratitude to the organization for providing the essential facilities at the Research Centre and AR&DB DRDO Research Lab, Department of Mechanical Engineering, SDM College of Engineering and Technology, Dharwad.

FUNDING

The authors extend their appreciation to the Deanship of Scientific Research at King Khalid University for funding this work through the Large Group Research Project under grant number RGP.2/622/46.

REFERENCES

[1] Arki, S., Ferrero, J.-F., Marguet, S., Redonnet, J.-M., Aury, A. (2019). Strengthening of a curved composite beam by introducing a flat portion, Compos. Struct., 222(110863), p. 110863. DOI: https://doi.org/10.1016/j.compstruct.2019.04.035.

[2] Wu, T., Zhou, G., Cai, D., Zhou, F., Cai, L. (2021). Effect of internal heating on delamination properties of deicing composite curved beams under four-point bending, Compos. Struct., 256(113084), p. 113084. DOI: https://doi.org/10.1016/j.compstruct.2020.113084.

[3] Dinesh Babu, V., Arumugam, V., Santulli, C. (2023). Experimental investigation of the enhancement of delamination resistance in glass/epoxy curved laminates, J. Mater. Sci., 58(37), pp. 14723–14739. DOI: https://doi.org/10.1007/s10853-023-08954-x.

[4] Ranz, D., Cuartero, J., Miravete, A., Miralbes, R. (2017). Experimental research into interlaminar tensile strength of carbon/epoxy laminated curved beams, Compos. Struct., 164, pp. 189–197. DOI: https://doi.org/10.1016/j.compstruct.2016.12.010.

[5] Ju, H., Nguyen, K.-H., Chae, S.-S., Kweon, J.-H. (2017). Delamination strength of composite curved beams reinforced by grooved stainless-steel Z-pins, Compos. Struct., 180, pp. 497–506. DOI: https://doi.org/10.1016/j.compstruct.2017.08.018.

[6] Gong, B., Ouyang, W., Nartey, M., Wang, H., Potter, K.D., Peng, H.-X. (2020). Minimizing the in-plane damage of Z-pinned composite laminates via a pre-hole pin insertion process, Compos. Sci. Technol., 200(108413), p. 108413. DOI: https://doi.org/10.1016/j.compscitech.2020.108413.

[7] Ashok., Uppin, V.S., Huddar, D.S., Kodancha, K.G., Sridhar, I., Shivakumar Gouda, P.S. (2016). Investigation on pseudo-ductility to improve mechanical behavior in glass-cellulose epoxy composites, IOP Conf. Ser. Mater. Sci. Eng., 149, p. 012112. DOI: https://doi.org/10.1088/1757-899x/149/1/012112.

[8] Uppin, V.S., Ashok., Joshi, A., Sridhar, I., Shivakumar Gouda, P.S. (2016). Interlaminar Fracture toughness in Glass-Cellulose Reinforced Epoxy hybrid composites, IOP Conf. Ser. Mater. Sci. Eng., 149, p. 012113. DOI: https://doi.org/10.1088/1757-899x/149/1/012113.

[9] Kiran, M.D., Govindaraju, H.K., Kumar, N., Nagaral, M., Khankal, D.V., Pandhare, A.P., Babu, E.R., Anjinappa, C., Razak, A., Wodajo, A.W. (2024). Effect of CNT filler and temperature on fracture toughness of epoxy composites reinforced with carbon fabric, Eng. Rep., 6(8). DOI: https://doi.org/10.1002/eng2.12816.

[10] Venkatesan, D.B., Vellayaraj, A., Chelliah, S.K. (2024). The influence of thickness and recycled milled glass fiber fillers on the delamination resistance of polymer composite angle brackets, Polym. Compos., 45(4), pp. 3067–3080. DOI: https://doi.org/10.1002/pc.27971

[11] Shivakumar Gouda, P.S., Sridhar, I., Umarfarooq, M.A. (2022). Crack suppression in glass epoxy hybrid L-bend composites through drawdown coating technique using nano and micro fillers, Mater. Today, 62, pp. 7292–7296. DOI: https://doi.org/10.1016/j.matpr.2022.04.465.

[12] Gumgol, U., Umarfarooq, M.A., Huddar, D., Vastrad, J.V., Wilkinson, A., Shivakumar Gouda, P.S. (2019). Influence of Kenaf and GO on interlaminar radial stresses in glass/epoxy L-bend laminates, SN Appl. Sci., 1(1).

DOI: https://doi.org/10.1007/s42452-018-0108-6.
[13] Gumgol, U., Huddar, D., Gouda, A., Vastrad, J.V., Veeresh Kumar, G.B., Wilkinson, A., Shivakumar Gouda, P.S. (2018). Interlaminar stresses in glass-cellulose epoxy L bend hybrid composites, Mater. Today, 5(11), pp. 24846–24853. DOI: 10.1016/j.matpr.2018.10.283.
[14] Avalon, S.C., Donaldson, S.L. (2011). Strength of composite angle brackets with multiple geometries and nanofiber-enhanced resins, J. Compos. Mater., 45(9), pp. 1017–1030. DOI: https://doi.org/10.1177/0021998310381538.
[15] Arca, M.A., Coker, D. (2014). Experimental investigation of CNT effect on curved beam strength and interlaminar fracture toughness of CFRP laminates, J. Phys. Conf. Ser., 524, p. 012038. DOI: https://doi.org/10.1088/1742-6596/524/1/012038.
[16] Levy-Wendt, B.L., Bever, A.M., Wright, N.C., Venable, T.J., Dally, J.P., Shih, F.J. (2014). Interlaminar tensile strength of CFRP composites reinforced with interleaved carbon nanotube sheets., Volume 14: Emerging Technologies; Engineering Management, Safety, Ethics, Society, and Education; Materials: Genetics to Structures, American Society of Mechanical Engineers.
[17] Wang, S., Akbolat, M.Ç., Katnam, K.B., Zou, Z., Potluri, P., Sprenger, S., Taylor, J. (2022). On the R-curve behaviour of carbon/epoxy laminates with core-shell rubber nanoparticle and micro-fibre veil hybrid toughening: Carbon vs PPS veils, Polymer (Guildf.), 254(125081), p. 125081. DOI: https://doi.org/10.1016/j.polymer.2022.125081.
[18] Wang, J., Ma, C., Chen, G., Dai, P. (2020). Interlaminar fracture toughness and conductivity of carbon fiber/epoxy resin composite laminate modified by carbon black-loaded polypropylene non-woven fabric interleaves, Compos. Struct., 234(111649), p. 111649. DOI: https://doi.org/10.1016/j.compstruct.2019.111649.
[19] Nagi, C.S., Ogin, S.L., Mohagheghian, I., Crean, C., Foreman, A.D. (2020). Spray deposition of graphene nano-platelets for modifying interleaves in carbon fibre reinforced polymer laminates, Mater. Des., 193(108831), p. 108831. DOI: https://doi.org/10.1016/j.matdes.2020.108831.
[20] Zhou, H., Du, X., Liu, H.-Y., Zhou, H., Zhang, Y., Mai, Y.-W. (2017). Delamination toughening of carbon fiber/epoxy laminates by hierarchical carbon nanotube-short carbon fiber interleaves, Compos. Sci. Technol., 140, pp. 46–53. DOI: https://doi.org/10.1016/j.compscitech.2016.12.018.
[21] Quan, D., Farooq, U., Zhao, G., Dransfeld, C., Alderliesten, R. (2022). Recycled carbon fibre mats for interlayer toughening of carbon fibre/epoxy composites, Mater. Des., 218(110671), p. 110671. DOI: https://doi.org/10.1016/j.matdes.2022.110671.
[22] Gheryani, A.A., Fleming, D.C., Reichard, R.P. (2019). Nonwoven polyester interleaving for toughness enhancement in composites, J. Compos. Mater., 53(28–30), pp. 4349–4367. DOI: https://doi.org/10.1177/0021998319857116.
[23] Uppin, V.S., Shivakumar Gouda, P.S., Sridhar, I., Umarfarooq, M.A., Edacherian, A. (2024). Effects of carbon/glass nonwoven interleaving veils and their areal density on opening and shearing mode interlaminar fracture toughness of glass epoxy composites, Theor. Appl. Fract. Mech., 130(104292), p. 104292. DOI: https://doi.org/10.1016/j.tafmec.2024.104292.
[24] Yang, S., Meninno, C., Chalivendra, V., Kim, Y. (2020). Electro-bending behavior of curved natural fiber laminated composites, Compos. Struct., 238(112004), p. 112004. DOI: https://doi.org/10.1016/j.compstruct.2020.112004.
[25] D30 Committee. (2022). Test method for measuring the curved beam strength of a fiber-reinforced polymer-matrix composite, West Conshohocken, PA, ASTM International.
[26] Lekhnitskii, S.G., (1968). Chapter IX. Theory of Bending of Anisotropic Plates (thin plates). Anisotropic Plates, Gordon and Breach, Science Publishers, New York, USA, pp.533.
[27] Umarfarooq, M.A., Gouda, P.S.S., Bharath, K.N., Veereshkumar, G.B., Banapurmath, N.R., Edacherian, A. (2022). Effects of residual stresses on interlaminar radial strength of Glass-Epoxy L-bend composite laminates, Frat. Integrità Strutt., 16(61), pp. 140–153. DOI: https://doi.org/10.3221/igf-esis.61.10.